



# Anthropogenic CO<sub>2</sub> emission reduction during the COVID-19 pandemic in Nanchang City, China<sup>☆</sup>

Cheng Hu <sup>a,b,1,\*</sup>, Timothy J. Griffis <sup>c</sup>, Lingjun Xia <sup>d,1</sup>, Wei Xiao <sup>e</sup>, Cheng Liu <sup>f</sup>, Qitao Xiao <sup>g</sup>, Xin Huang <sup>h</sup>, Yanrong Yang <sup>a</sup>, Leying Zhang <sup>a</sup>, Bo Hou <sup>a</sup>

<sup>a</sup> College of Biology and the Environment, Joint Center for Sustainable Forestry in Southern China, Nanjing Forestry University, Nanjing, 210037, China

<sup>b</sup> Collaborative Innovation Center on Forecast and Evaluation of Meteorological Disasters (CIC-FEMD), Nanjing University of Information Science & Technology, Nanjing, China

<sup>c</sup> Department of Soil, Water, and Climate, University of Minnesota-Twin Cities, St. Paul, Minnesota, USA

<sup>d</sup> Ecological Meteorology Center, Jiangxi Meteorological Bureau, Nanchang, 330096, China

<sup>e</sup> Yale-NUIST Center on Atmospheric Environment, International Joint Laboratory on Climate and Environment Change (ILCEC), Nanjing University of Information, Science & Technology, Nanjing, 210044, China

<sup>f</sup> Jiangxi Province Key Laboratory of the Causes and Control of Atmospheric Pollution/School of Water Resources and Environmental Engineering, East China University of Technology, Nanchang, 330013, China

<sup>g</sup> Key Laboratory of Watershed Geographic Sciences, Nanjing Institute of Geography and Limnology, Chinese Academy of Sciences, Nanjing, 210008, China

<sup>h</sup> Key Laboratory of Eco-Environmental and Meteorology for the Qinling Mountains and Loess Plateau, Shaanxi Meteorological Bureau, Xi'an, 710014, Shaanxi, China

## ARTICLE INFO

### Keywords:

WRF-STILT model  
City scale  
Top-down method  
Bayesian inversion method

## ABSTRACT

China is the largest CO<sub>2</sub> emitting country on Earth. During the COVID-19 pandemic, China implemented strict government control measures on both outdoor activity and industrial production. These control measures, therefore, were expected to significantly reduce anthropogenic CO<sub>2</sub> emissions. However, large discrepancies still exist in the estimated anthropogenic CO<sub>2</sub> emission reduction rate caused by COVID-19 restrictions, with values ranging from 10% to 40% among different approaches. Here, we selected Nanchang city, located in eastern China, to examine the impact of COVID-19 on CO<sub>2</sub> emissions. Continuous atmospheric CO<sub>2</sub> and ground-level CO observations from January 1st to April 30th, 2019 to 2021 were used with the WRF-STILT atmospheric transport model and *a priori* emissions. And a multiplicative scaling factor and Bayesian inversion method were applied to constrain anthropogenic CO<sub>2</sub> emissions before, during, and after the COVID-19 pandemic. We found a 37.1–40.2% emission reduction when compared to the COVID-19 pandemic in 2020 with the same period in 2019. Carbon dioxide emissions from the power industry and manufacturing industry decreased by 54.5% and 18.9% during the pandemic period. The power industry accounted for 73.9% of total CO<sub>2</sub> reductions during COVID-19. Further, emissions in 2021 were 14.3–14.9% larger than in 2019, indicating that economic activity quickly recovered to pre-pandemic conditions.

## 1. Introduction

China has promised to reach a carbon emission peak by 2030 and carbon neutralization by 2060. To reach these ambitious goals, there is a need to provide accurate understanding of anthropogenic CO<sub>2</sub> emissions from city to province scales, but the large uncertainty (>50%) in most state-of-the-art inventories (i.e. for years 2010–2018) at city scales may

hinder this ambitious goal (Seto et al., 2014; Han et al., 2020a). To prevent the spread of the coronavirus (COVID-19), China imposed strict control measures, which indirectly triggered a large lockdown on both fossil fuel consumption and corresponding CO<sub>2</sub> emissions. The unintentional reduction of fossil fuel use provides a unique opportunity to investigate how government measures can be used to reduce anthropogenic emissions and to evaluate the uncertainty between different

<sup>☆</sup> This paper has been recommended for acceptance by Admir Créo Targino.

\* Corresponding author. College of Biology and the Environment, Joint Center for Sustainable Forestry in Southern China, Nanjing Forestry University, Nanjing, 210037, China.

E-mail addresses: [nihaochuheng@163.com](mailto:nihaochuheng@163.com), [chenghu@njfu.edu.cn](mailto:chenghu@njfu.edu.cn) (C. Hu).

<sup>1</sup> Cheng Hu and Lingjun Xia contribute equally.

emission estimation approaches.

Some pioneering research has used different approaches to quantify the spatiotemporal changes of CO<sub>2</sub> emission reductions during the COVID-19 pandemic in 2020. These studies provide the most recent assessments of CO<sub>2</sub> reduction and have been made available to the public and policy makers (Turner et al., 2020; Liu et al., 2020; Liu et al., 2020; Weir et al., 2021). Some of these investigations focused on or included parts of China (Liu et al., 2020; Han et al., 2020b; Huang et al., 2021; Wu et al., 2021; Zheng et al., 2020a, 2020b; Zeng et al., 2022). However, many of these studies have evaluated anthropogenic reductions over different periods of time (i.e., from January–April or a portion of this period). Large discrepancies exist in the rates of reduced CO<sub>2</sub> emission during COVID-19 pandemic with mean values varying from 10 to 40% (four-fold) in eastern China, which accounted for more than half of the Nation's Gross Domestic Product (GDP) and greenhouse gas emissions (Liu et al., 2020; Han et al., 2020b; Huang et al., 2021; Zheng et al., 2020b).

These discrepancies exist not only between top-down and bottom-up approaches, but among the same bottom-up methods. Recent work by Huang et al. (2021) used city-level activity data and specific sector information and concluded that CO<sub>2</sub> emissions were reduced by 40% in eastern China. They estimated that CO<sub>2</sub> emissions were reduced by about 4 times that reported by Han et al. (2020b) who used GDP data as a proxy. Han et al. (2020b) estimated that CO<sub>2</sub> emissions were reduced by 11% in China and eastern China. Le Quéré et al. (2020) also used activity data to calculate global anthropogenic CO<sub>2</sub> reductions, and found less than a 20% reduction for eastern China. These large discrepancies result from the availability of activity data, representativeness of proxy data, and the disaggregation of GHG emission calculations within scope1-3 (Gurney et al., 2021; Mueller et al., 2021). Taking traffic CO<sub>2</sub> emissions as an example, human mobility data was used instead of traffic fossil use in calculating changes in CO<sub>2</sub> emissions during the COVID-19 pandemic (He et al., 2020; Le Quéré et al., 2020). Recent work suggests a large relative emission bias of -20–13% when using such data (Oda et al., 2021). Another study found a relative bias of 60% when compared to results using mobility as a proxy for traffic data (Gensheimer et al., 2021). Hence, questions still remain when evaluating these bottom-up approaches, as to whether these results are comprehensive, accurate and comparable between different cities or countries.

Atmospheric CO<sub>2</sub> concentration observations within the planetary boundary layer (PBL) are considered to be more sensitive to emission changes than column averages, and can provide timely insight and independent evaluation of bottom-up and satellite type approaches (Basu et al., 2020). The coupling of atmospheric transport models with high precision CO<sub>2</sub> concentration observations can be used to constrain sector- and source-specific emissions for a target area, which has been widely used in greenhouse gas emission studies for urban areas (Turner et al., 2020; Hu et al., 2019, 2021). To the best of our knowledge, there are no studies that have combined atmospheric transport models with CO<sub>2</sub> concentration observations to quantify the impact of COVID-19 pandemic on city scale anthropogenic CO<sub>2</sub> emissions in China. Further, a robust and independent evaluation is needed to reduce the large uncertainties and discrepancies reported for bottom-up approaches.

Atmospheric CO<sub>2</sub> inversions can be compared with other atmospheric tracers to provide independent constraints on the CO<sub>2</sub> emissions. Among key urban pollution species (i.e. PM<sub>2.5</sub>, SO<sub>2</sub>, NO<sub>x</sub>, CO, O<sub>3</sub>), carbon monoxide (CO) is an excellent tracer for understanding CO<sub>2</sub> emissions because CO is mainly emitted by the incomplete combustion of fossil fuel including coal, diesel and natural gas, with similar sources as anthropogenic CO<sub>2</sub> emissions. Consequently, the atmospheric CO can provide independent evidence of changes in anthropogenic CO<sub>2</sub> emissions that occurred during the COVID-19 pandemic.

To quantify how government control measures have reduced anthropogenic CO<sub>2</sub> emissions during the COVID-19 pandemic in 2020

and assess whether it rebounded in 2021, we conducted three years of atmospheric CO<sub>2</sub> observations from 2019 to 2021 on a 50-m tower and used ground-level CO observations in the urban area of Nanchang city, located in eastern China. The tower-based CO<sub>2</sub> observations is the closest CO<sub>2</sub> observation site to Wuhan city, which was the reported outbreak area of COVID-19 cases in China. Here, we couple *a priori* emissions with transport modeling and concentration observations to (1) quantify anthropogenic CO<sub>2</sub> emission changes during, before, and after the COVID-19 pandemic and (2) analyze the contributions from different emission categories to total CO<sub>2</sub> emission changes.

## 2. Measurement and modeling framework

### 2.1. Atmospheric CO<sub>2</sub> and CO observations

Carbon dioxide concentrations were measured on a tower at 50 m above the ground. The tower is located in Nanchang city (hereafter NC site, 28°41' N, 115°46' E, black cross in Fig. 1), the capital of Jiangxi province and is 250 km from Wuhan city. Atmospheric CO<sub>2</sub> is continuously measured using a Cavity Ring-Down Spectroscopy (CRDS) system (model G2401, Picarro Inc, Sunnyvale, CA), with two air sampling inlets positioned at 50 m and 30 m above ground. To ensure high precision observations, the measurement systems were calibrated every 2 h with standard gases traceable to NOAA/GML (NOAA Global Monitoring Laboratory) standards (see calibration details in Supplementary Material, Section S1). The precision of the hourly CO<sub>2</sub> observations is 0.1 ppm (Fang et al., 2014; Hu et al., 2021). In this study, we have used the 50 m height data to take advantage of its larger source footprint area.

The CO observations were conducted and provided by the China National Environmental Monitoring Center (<http://datacenter.mep.gov.cn/>, last accessed: 17 May 2021). Site information for Nanchang city is listed in Table S1. We averaged all CO observation sites within the boundary of Nanchang city before comparison with the CO simulations.

### 2.2. Local government control measures

Governments of the local and surrounding provinces enacted a Level 1 response from January 24th, 2020 to March 12th, 2020, during which most factories and construction activities were suspended and traffic was substantially restricted. These restrictions were then reduced to Level 2 from March 13th, and then to Level 3 from March 20th. These reduced restrictions resulted in significant recovery of the economic and industrial activity to near-normal conditions. We combined Level 2 and 3 periods as Level 2–3 from March 13th to April 30th. Hence both Level 1 and Level 2–3 periods span approximately 50 days. We treat the year 2019 as the baseline year and compared year 2020 with 2019 to quantify government control measures on CO<sub>2</sub> emissions during the COVID-19 pandemic. We also compared year 2021 with 2019 to quantify the emission changes after the social and economic activity recovered to normal conditions.

### 2.3. WRF-STILT model setup

Two nested domains were used to simulate meteorological fields in the Weather Research and Forecasting Model (WRF version 4.2.2). The outer nested domain (D1, 27 km × 27 km grid resolution, Fig. S1) covers eastern and central China, and the inner domain (D2, 9 km × 9 km grid resolution) covers central China. The physical schemes used in the WRF model are the same as those used in our previous studies (Hu et al., 2019, 2021) and are described in the Supplementary Material. We also evaluated these meteorological fields with five sites (Fig. S2, Section S2). These simulated meteorological fields are used to drive the Stochastic Time-Inverted Lagrangian Transport (hereafter STILT) model to simulate the concentration footprint with spatial resolution of 0.1° × 0.1° and a temporal resolution of 1 h. The concentration footprint represents the sensitivity of the concentration changes to its regional sources/sinks.

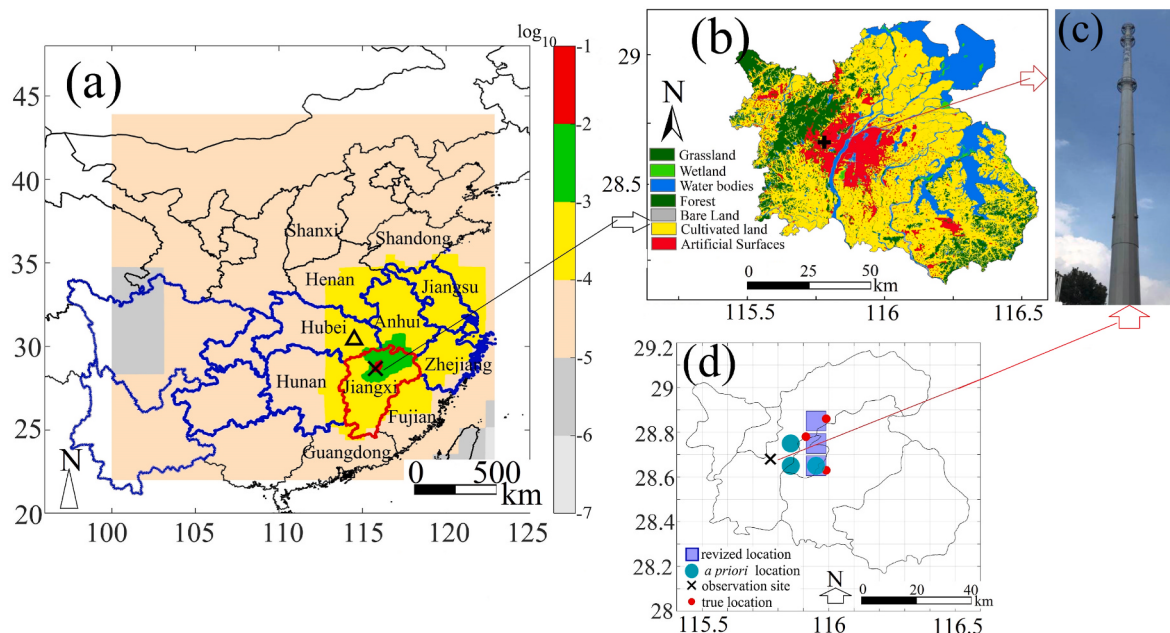


**Fig. 1.** (a) Mean footprint from January to April in three years (2019, 2020 and 2021), symbol “ $\times$ ” indicates  $\text{CO}_2$  observation site and “ $\Delta$ ” is location of Wuhan city, the units for footprint:  $\text{ppm m}^2 \text{s mol}^{-1}$ , (b) land use in Nanchang city, (c) tower of atmospheric  $\text{CO}_2$  concentration observation, and (d) location mismatch of three power industry facilities within the boundary of Nanchang city, “true location”, “*a priori* location” “revised location” represent the real location of three power industry facilities based on google map search, locations in EDGAR inventory, locations in EDGAR v6.0 inventory.

The concentration enhancement is calculated by multiplying the source footprint with the flux (Hu et al., 2019, 2021). Note that the footprint for each hourly enhancement was simulated by releasing 500 air particles per hour for 7 days. The WRF-STILT framework tracks the locations and time each particle remained within the PBL until the particles leave the outer domain. Therefore, the simulation of each hourly enhancement contains information from 168 hourly footprints, which represents 7 days of atmospheric transport processes. In the model framework, atmospheric  $\text{CO}_2$  (or  $\text{CO}$ ) at a given site is equal to a background value when air flow enters into the study domain and an enhancement, which includes contribution from local sources or sinks. Here, we treat sources as positive enhancements and sinks as negative enhancements (i.e. plant photosynthesis for  $\text{CO}_2$  and reaction with hydroxyl radical for  $\text{CO}$ ).

#### 2.4. The *a priori* $\text{CO}_2$ and $\text{CO}$ flux

The *a priori* anthropogenic  $\text{CO}_2$  and  $\text{CO}$  emissions used in this study are from the Emission Database for Global Atmospheric Research (EDGAR), which provides monthly mean global anthropogenic  $\text{CO}_2$  and  $\text{CO}$  emissions with spatial resolution of  $0.1^\circ$  (Fig. 3a–b). The v6.0  $\text{CO}_2$  inventory is for the year 2018, and the most recent v5.0  $\text{CO}$  inventory is for the year 2015. EDGAR v6.0 contains 28 categories of anthropogenic  $\text{CO}_2$  emissions with 19 categories for fossil fuel related combustion and 9 categories for biomass related combustion. To derive hourly  $\text{CO}_2$  emissions, we applied hourly scaling factors for the main emission categories as displayed in Fig. 3c. Details of the *a priori*  $\text{CO}_2$  (or  $\text{CO}$ ) inventory and concentration simulation framework are introduced in the Supplementary Material (Section S3–S4).

Compared with the true locations of each  $\text{CO}_2$  emission facility (especially for  $\text{CO}_2$  hotspots), the location mismatch in EDGAR inventories have been reported in previous studies and can potentially lead to large discrepancies of simulated  $\text{CO}_2$  enhancement when the observation site is near these facilities (Zavala-Araiza et al., 2015; Paris et al., 2021). We conducted a detailed local survey of the spatial distributions for power industry facilities and found a spatial mismatch of three facilities with corresponding locations in the EDGAR v6.0 inventory within the boundary of Nanchang city. Hence, we have changed

their locations to match the true locations as shown in Fig. 1d.

#### 2.5. Inverse modeling: bayesian inversion method

To provide robust results, two atmospheric inversion methods are used to constrain  $\text{CO}_2$  emissions. We first applied a Bayesian inversion method to interpret the atmospheric  $\text{CO}_2$  observation changes in terms of quantitative constraint on anthropogenic  $\text{CO}_2$  emissions and its components for different periods. The optimal solution in this method is to minimize a cost function  $J(\Gamma)$ , which represents the mismatch between  $\text{CO}_2$  observations and simulations and the mismatch between *posteriori* and *a priori* scaling factors (hereafter SF) (Miller et al., 2008; Griffis et al., 2017). The cost function  $J(\Gamma)$  is expressed as:

$$J(\Gamma) = \frac{1}{2}[(y - K\Gamma)^T S_e^{-1} (y - K\Gamma) + (\Gamma - \Gamma_a)^T S_a^{-1} (\Gamma - \Gamma_a)] \quad (1)$$

where  $y$  represents the vector of observed  $\text{CO}_2$  enhancement,  $K$  is the Jacobian matrix which defines the sensitivities of observations to corresponding source contributions,  $\Gamma$  is the state vector to be optimized and consists of the *posteriori* SFs for the various source contributions,  $S_e$  and  $S_a$  are the error covariance matrices for observations and the *a priori* values, where  $S_e$  consists of measurement and model errors. Here  $\Gamma_a$  is treated as 1. The solution for minimizing the cost function  $J(\Gamma)$  and obtaining the *posteriori* SFs is to solve  $\nabla_{\Gamma} J(\Gamma) = 0$ , and is given by,

$$\Gamma_{\text{post}} = (K^T S_e^{-1} K + S_a^{-1})^{-1} (K^T S_e^{-1} y + S_a^{-1} \Gamma_a) \quad (2)$$

Prior to solving  $\nabla_{\Gamma} J(\Gamma) = 0$ , the Bayesian inversion method requires an estimate of the error covariance matrices and the state vector for the *a priori* and observational data. The measurement errors ( $S_{\text{obs}}$ ) include the enhancement uncertainty (10%, which is mainly attributed to the uncertainty in the background values as discussed in Hu et al. (2019)). As illustrated in our previous studies (Hu et al., 2019; Griffis et al., 2017; Chen et al., 2016), the uncertainty in simulated  $\text{CO}_2$  enhancement can be caused by WRF-STILT model errors, where two primary sources of model errors arise from (1) the finite number of particles released in the STILT model ( $S_{\text{particles}}$ ) and uncertainty in meteorological fields,

especially for boundary layer height simulations ( $S_{\text{met}}$ ).

We assigned a relative uncertainty of 13% for  $S_{\text{particles}}$ , which accounts for the uncertainties associated with releasing a finite number (i.e. 500) of particles to simulate the concentration source footprint (Miller et al., 2008; Griffis et al., 2017; Chen et al., 2016). A previous study for an agricultural area in the Midwest U.S.A. used an uncertainty of 21% in simulating planetary boundary layer height (Chen et al., 2016). Considering that our study area is located in a more complex urban landscape, the high inhomogeneity for urban buildings may not be well resolved in the model domain and can potentially cause larger biases in wind profiles and boundary layer height simulations. The relative bias of the simulated 10 m wind speed was approximately 30% and a recent study found that daytime bias in PBLH reanalysis products can reach up to 40% in China (Guo et al., 2017). Therefore, we assigned uncertainty values of 30% and 40% for  $S_{\text{met}}$ . Recent work suggests an uncertainty in the *a priori* anthropogenic CO<sub>2</sub> emission inventory in China of about 50% at the city scale (Han et al., 2020a). We assigned a value of 50% to the emission uncertainty during the Level 2–3 periods. Because emission reduction in the Level 1 period are considered much larger caused by government control measures, we assigned both 50% and 100% for its uncertainty for the Level 1 period, which aims to test the sensitivity of inversion results to the relative uncertainty prescribed for the *a priori* estimates. The uncertainty in the biological CO<sub>2</sub> flux related to the Carbon Tracker product has not yet been reported. Here, we estimate it based on the relative difference of biological CO<sub>2</sub> among different NEE products to test its sensitivity. To assess whether the emission constraint results are sensitive to the above uncertainties, we conducted different uncertainty tests including 8 cases for the Level 1 period and 4 cases for the Level 2–3 periods as shown in Table S2.

## 2.6. Inverse modeling: multiplicative scaling factor method

We also used the multiplicative scaling factor (hereafter MSF) method, which has been applied broadly to constrain greenhouse gas and other tracer gas emissions. The MSF SFs were derived by dividing the observed enhancement by the simulated enhancement (Sargent et al., 2018; He et al., 2020),

$$SF(CO_2) = \frac{CO_{2,\text{obs}} - CO_{2,\text{bg}} - \Delta CO_{2,\text{bio}}}{\Delta CO_{2,\text{anthro}}} \quad (3)$$

where SF(CO<sub>2</sub>) is the scaling factor and CO<sub>2,obs</sub>, CO<sub>2,bg</sub>, ΔCO<sub>2,bio</sub> and ΔCO<sub>2,anthro</sub> are the CO<sub>2</sub> concentration observations, background CO<sub>2</sub>, simulated biological CO<sub>2</sub> concentration, and simulated anthropogenic CO<sub>2</sub> enhancement, respectively. The details of how to calculate CO<sub>2,obs</sub>, CO<sub>2,bg</sub>, ΔCO<sub>2,bio</sub> and ΔCO<sub>2,anthro</sub> are provided in the Supplementary Material (Section S3).

## 3. Results and discussion

### 3.1. Analysis of atmospheric CO<sub>2</sub> concentration

Atmospheric CO<sub>2</sub> variations are mainly influenced by meteorological fields, background, anthropogenic emissions, and sinks/sources from ecosystems. Although the direct comparison of CO<sub>2</sub> concentration between different periods cannot solely reflect regional CO<sub>2</sub> emission changes, they carry some essential information about emission changes over longer periods. To illustrate the influence of government control measures on CO<sub>2</sub> emissions, we first examined the daily CO<sub>2</sub> concentration variations from January 1st to April 30th for years 2019–2021 (Fig. 2a–c). One important difference was that CO<sub>2</sub> concentrations were generally below 440 ppm in 2020, and higher than 440 ppm in 2019 and 2021. The mean concentrations during the Level 1 period were 442.4 ppm, 436.3 ppm and 449.0 ppm for year 2019, 2020 and 2021, respectively, and the standard deviations were 9.2 ppm, 8.0 ppm, and 12.4 ppm in the respective years. For the Level 2–3 periods, the mean values were 439.9 ppm, 437.5 ppm and 450.1 ppm, and standard deviations were 12.9 ppm, 11.1 ppm and 12.9 ppm for the respective years. These results indicated that CO<sub>2</sub> concentrations were significantly lower ( $P < 0.01$ ) during the Level 1 period (COVID-19 pandemic) in 2020 when compared with the other two years. The CO<sub>2</sub> concentration had not recovered to pre-pandemic values in Level 2–3 even though government policies were relaxed to help support the local economy. Another difference appeared after the Chinese Spring Festival that showed the CO<sub>2</sub> concentration kept this trend for a longer time in 2020 than years 2019 and 2021. This can be explained by the fact that the

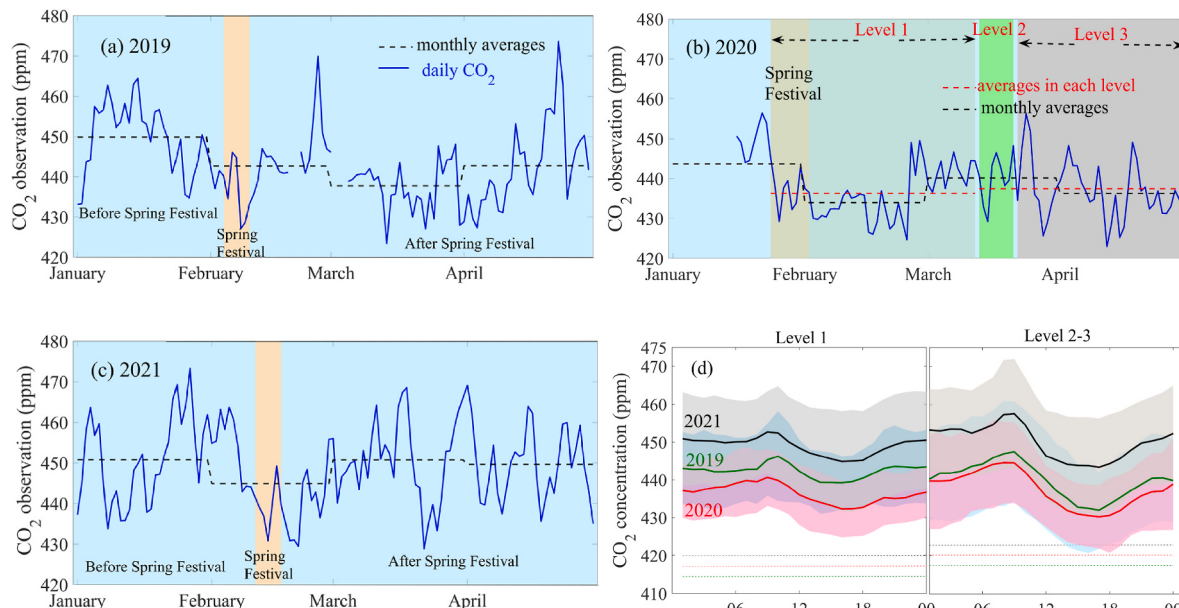


**Fig. 2.** Time series of daily CO<sub>2</sub> observations from January to April for years (a) 2019, (b) 2020, (c) 2021, and (d) diel averages of CO<sub>2</sub> observations. Note the different background color in panel a–c represents corresponding periods as labeled, the black dashed lines represent monthly averages and red dashed lines are averages in each level during 2020, dash line in panel d is CO<sub>2</sub> background. (For interpretation of the references to color in this figure legend, the reader is referred to the Web version of this article.)

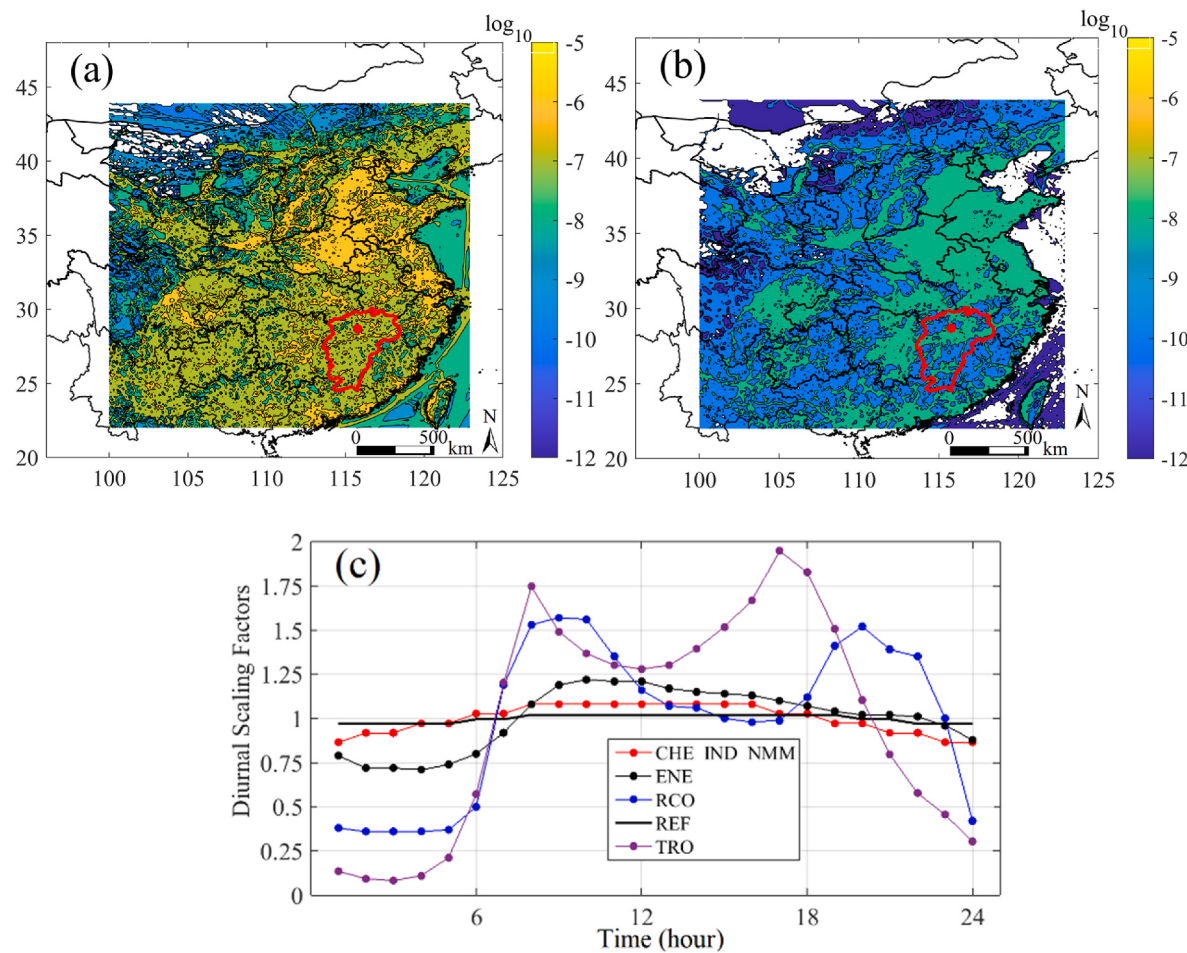


**Fig. 3.** (a) Anthropogenic CO<sub>2</sub>, (b) CO emission averages from January to April (units: mol m<sup>-2</sup> s<sup>-1</sup>), (c) hourly variations for different anthropogenic CO<sub>2</sub> sectors.

government in most provinces began to execute strict stay home rules to the middle of March, which limited both private outdoor activities and work in factories.

Diel averages for atmospheric CO<sub>2</sub> observations from 2019 to 2021 are displayed in Fig. 2d. The comparisons between 2020 and the other two years show a significant decrease ( $P < 0.01$ ) in 2020, providing additional support that CO<sub>2</sub> emissions were reduced substantially by the COVID-19 pandemic and corresponding government regulations. We also found that CO<sub>2</sub> observations in 2021 showed a large increase compared to both 2019 and 2020, which reflects the economic recovery and anthropogenic CO<sub>2</sub> emission increase. The CO<sub>2</sub> enhancements (i.e. observations minus background values, Fig. S3) contain direct regional emission information. Here, we have subtracted the annual increase of the global CO<sub>2</sub> background to illustrate the average enhancement values of 19.2 ppm for the Level 1 period and 17.3 ppm for Level 2–3 periods in year 2020. These values were 27.9 ppm and 22.5 ppm in 2019, and 29.1 ppm and 27.2 ppm in 2021, respectively. The CO<sub>2</sub> enhancements are influenced by both meteorological factors and sinks and sources (Hu et al., 2021). Later, we will use these observations with an atmospheric transport model to evaluate how anthropogenic emissions impacted the CO<sub>2</sub> concentrations with the region.

### 3.2. Comparisons between observed and simulated atmospheric CO<sub>2</sub>

The anthropogenic *a priori* CO<sub>2</sub> and CO emissions in Fig. 3a–b displayed similar spatial distributions and indicated similar emission sources. January–April averaged daily anthropogenic CO<sub>2</sub> emissions were  $9.5 \times 10^4$  tonnes for Nanchang city in the *a priori* EDGAR inventory. Here, to quantify how temporal profiles of emissions influence

the simulated atmospheric CO<sub>2</sub> (Section S5, Fig. 3c), we performed sensitivity tests and compared the differences between the simulated CO<sub>2</sub> enhancements from using both hourly versus constant anthropogenic CO<sub>2</sub> emissions. When considering the sum of all CO<sub>2</sub> enhancements (Fig. S4), the diel amplitude of these CO<sub>2</sub> variations changed over time because of variations in PBL height and wind fields. The use of temporal profiles indicates it can well represent the diel variations of CO<sub>2</sub> emissions and concentrations.

The mean concentration footprint of January to April for each year is displayed in Fig. 1a. We found that the area designated as green (mean footprint values larger than  $10^{-3}$  ppm m<sup>2</sup> s mol<sup>-1</sup>) was mainly located within Jiangxi province and represents higher sensitivity of CO<sub>2</sub> mixing ratio to these areas. The simulated relative proportions of CO<sub>2</sub> enhancement components, based on using the *a priori* emissions and emissions components from Nanchang city, are shown in Fig. S5 and Table S3. This demonstrates that simulated enhancement contributions from Nanchang city and the broader Jiangxi province accounted for 54.0% and 61.9% of the total enhancement, respectively. Contributions from other provinces are also discussed in Section S6 (Supplementary Material). The EDGAR v6.0 product showed that emissions from power industry, combustion for manufacturing, cement production, energy for building and the others accounted for 48.0%, 16.9%, 7.2%, 15.2% and 12.7%, respectively for Nanchang city. The simulated enhancements from these sources accounted for 53.4%, 15.7%, 5.9%, 15.4% and 9.6% of the total anthropogenic CO<sub>2</sub> enhancement. We note that on-road emissions accounted for only 2.46% of the anthropogenic CO<sub>2</sub> emissions in Nanchang city and the simulated enhancement accounted for 2.55% of the total anthropogenic enhancement. This contribution is very low when compared with the uncertainty of other source

categories. We found relatively good agreement of above values between simulated CO<sub>2</sub> enhancement and their emissions, and concluded that our observation site can represent emission components in Nanchang city. Further, to quantify the uncertainty in biological CO<sub>2</sub> flux, comparisons between three biological flux products from 2001 to 2018 are displayed in Fig. S6. The spatial-temporal relative differences were found to be larger than 100% (see Supplementary Materials Section S7 for further details).

Comparisons between observed and simulated hourly CO<sub>2</sub> concentrations are shown in Fig. 4. These data demonstrate that biological CO<sub>2</sub> enhancement plays a minor role in atmospheric CO<sub>2</sub> variations with mean of 1.7 ppm for year 2019 and 1.8 ppm for 2020. The statistical analysis of the root mean standard error (RMSE) was 15.9 ppm, mean bias (MB) was -2.5 ppm and correlation coefficient (R) was 0.28 for 2019. In 2020, the RMSE was 15.3 ppm, MB was 5.3 ppm, and R was 0.30. In 2021, the RMSE was 16.1 ppm, MB was -5.8 ppm, and R was 0.25. The difference between the model simulations and observations is likely caused by the following five factors: (1) bias in the *a priori* anthropogenic emissions; (2) COVID-19 caused anthropogenic CO<sub>2</sub> emission changes before, during and after mitigation periods that have not been accounted for in the *a priori* emission inventory; (3) all hourly data (including nighttime periods) for approximately 4 months was used to calculate the reported statistic, which can potentially reduce R values and increase MB because the nighttime transport uncertainty is relatively large compared to that at midday. For example, the statistical analysis when using only hourly midday concentrations indicates that the RMSE, MB and R were 13.5 ppm, -6.5 ppm, 0.39 for 2019, 11.0 ppm, 1.7 ppm and 0.40 for 2020, and 14.7 ppm, -8.5 ppm and 0.36 for 2021 and were improved when compared with using all-day concentration observations; (4) there are no emission height data in the EDGAR inventory. The STILT model treats all emissions as surface sources and does not assign their true emission heights. Therefore, strong point sources from tall stacks may lead to overestimation of simulated nighttime CO<sub>2</sub> concentration when the emission height is above the PBLH (Brunner et al., 2019); and (5) the uncertainty of atmospheric model transport for urban CO<sub>2</sub> emissions is much larger than in rural or agricultural regions because of the high heterogeneity of emissions associated with the urban environment. However, the time series of both hourly CO<sub>2</sub> observations and simulations in Fig. 4 shows that the WRF-STILT model can also capture the atmospheric CO<sub>2</sub> variations reasonably well over the majority of the study period especially for the Level 1 period in 2019. However, the observations in February 2020 were generally smaller than the simulations, indicating significant anthropogenic CO<sub>2</sub> emission reduction during the COVID-19 pandemic.

To better evaluate these biases, the diel averages of both CO<sub>2</sub> observations and simulations are displayed in Fig. 5a-f. In general, the bias in Figs. 4 and 5a-f was mainly caused by the *a priori* emission bias (or changes) and needs to be constrained by our tower CO<sub>2</sub> concentration observations as shown below. As mentioned above, most atmospheric inversion studies use midday CO<sub>2</sub> observations to constrain local anthropogenic CO<sub>2</sub> emissions because the midday PBL is typically well-mixed compared to at night. Further, the aggregation (or representation) error is also minimum at midday than at night with stable nocturnal conditions (Wang et al., 2022). Because the transport uncertainty is relatively small compared to that at night we have used the midday observations to constrain CO<sub>2</sub> emissions (see highlighted bold lines in Fig. 5a-f). For the year 2019, the observations were larger than the simulations for both periods, indicating potential underestimation of the *a priori* anthropogenic CO<sub>2</sub> emissions. In contrast to 2019, the observations in the Level 1 period of 2020 appeared to be smaller than the simulations, indicating an overestimation of *a priori* CO<sub>2</sub> emissions. This disparity can be explained by the strict control measures on both private and public activities during the COVID-19 pandemic. We also found that the observation-simulation mismatch in 2021 was much larger than in 2019, indicating rapid economic recovery in 2021 and, therefore, higher anthropogenic CO<sub>2</sub> emissions. Since GDP changes also reflects more (or less) energy need, especially for coal combustion power stations, the GDP data can be used as a proxy of anthropogenic CO<sub>2</sub> emission changes (Han et al., 2020b). We have examined GDP for Nanchang city and found that GDP varied from 12.96, 12.05, and 14.69 billion RMB in the first quarter of 2019, 2020 and 2021, respectively. These GDP data are consistent with the changes observed in CO<sub>2</sub> concentrations.

### 3.3. Constraint on anthropogenic CO<sub>2</sub> emissions

We first applied the multiplicative scaling factor method to derive *posteriori* anthropogenic CO<sub>2</sub> emissions during each period. Scaling factors (SFs) and the *posteriori* anthropogenic CO<sub>2</sub> emissions are listed in Table 1. The SFs were  $1.24 \pm 0.19$  for Level 1 period and  $1.26 \pm 0.10$  for Level 2-3 periods in 2019, and  $0.78 \pm 0.08$  and  $0.99 \pm 0.10$  in 2020, respectively. Because the *a priori* biological CO<sub>2</sub> flux for 2021 was not available, we used the biological CO<sub>2</sub> enhancement in 2019 for 2021. Here, the SFs were  $1.42 \pm 0.10$  for Level 1 period and  $1.41 \pm 0.10$  for Level 2-3 periods. When using the biological CO<sub>2</sub> enhancement in 2020 for 2021, the SFs were  $1.43 \pm 0.10$  and  $1.43 \pm 0.09$ . These results indicate that the biological enhancements did not significantly influence the scaling factors derived for these urban areas during the non-growing seasons. In summary, Table 1 illustrates that anthropogenic CO<sub>2</sub>

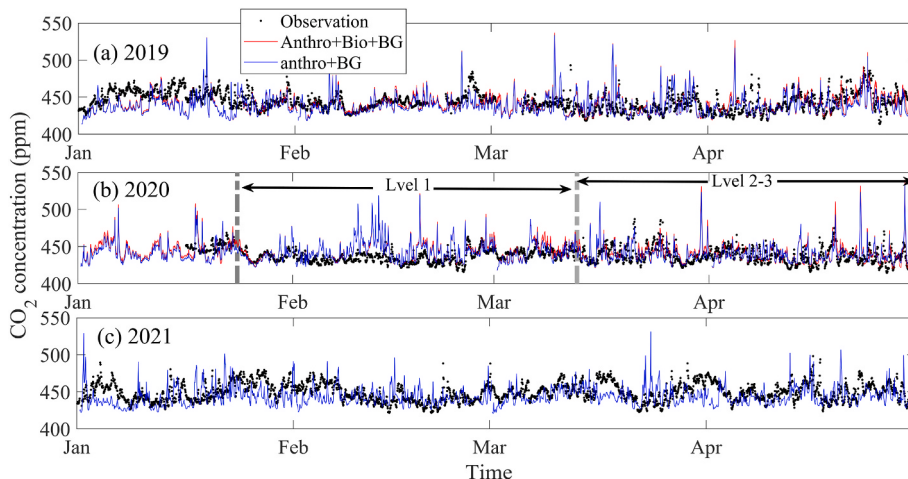


**Fig. 4.** Comparisons between hourly CO<sub>2</sub> observations and simulations from January to April in years (a) 2019, (b) 2020 and (c) 2021. Here “anthro + BG” represents the sum of simulated anthropogenic CO<sub>2</sub> enhancement and background, and “anthro + Bio + BG” represents the sum of simulated anthropogenic CO<sub>2</sub> enhancement, biological CO<sub>2</sub> enhancement and background.

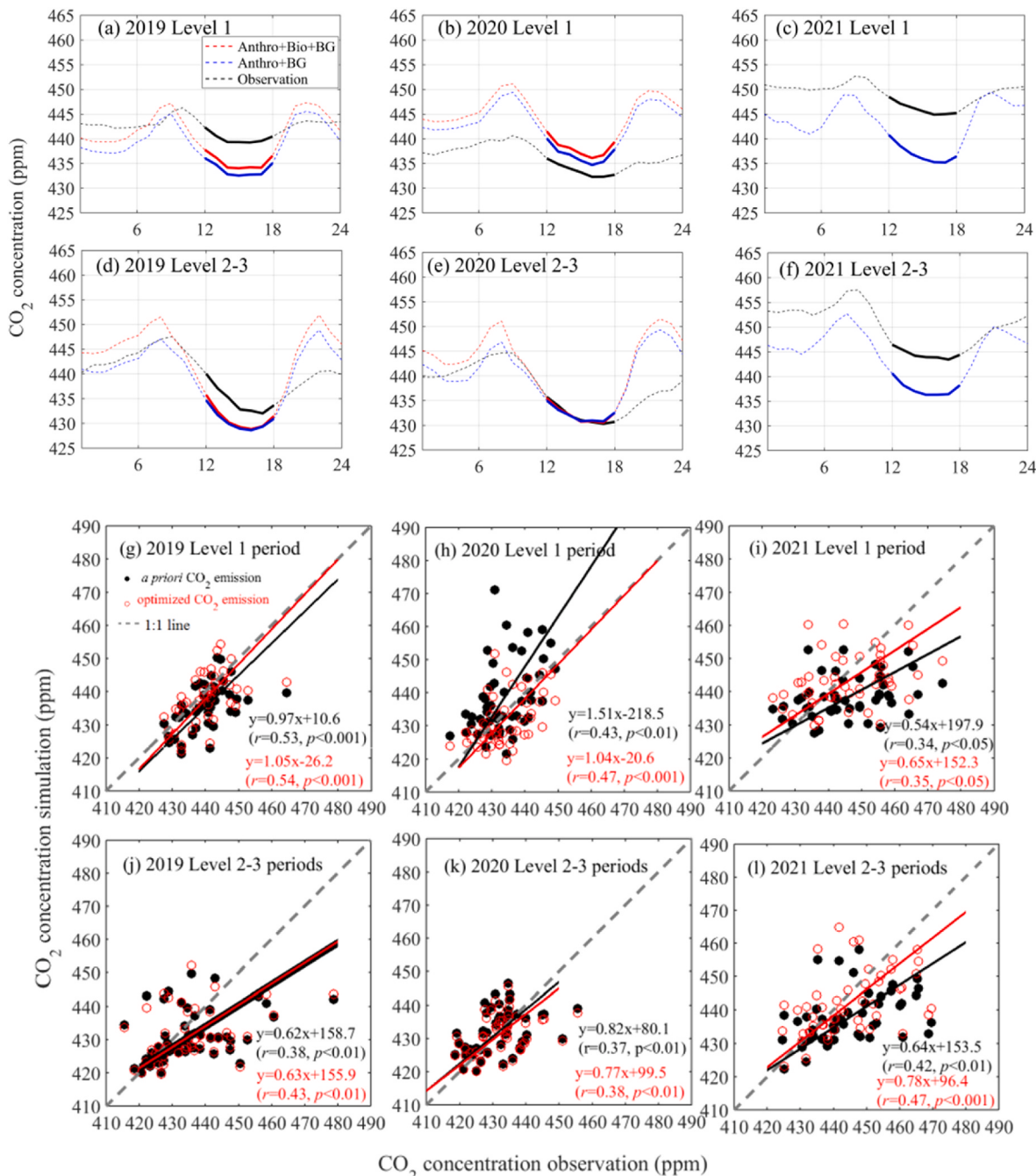


**Fig. 5.** Diel averages comparisons between observations and simulations for Level 1 period in (a) 2019, (b) 2020, (c) 2021, and Level 2–3 periods in (d) 2019, (e) 2020, and (f) 2021, midday (12:00–18:00, local time) values are displayed in bold lines. And comparisons between daily midday averages of CO<sub>2</sub> observations and simulated CO<sub>2</sub> concentrations using both *a priori* and optimized CO<sub>2</sub> emissions in corresponding periods (g)–(l). Here “anthro + BG” represents the sum of simulated anthropogenic CO<sub>2</sub> enhancement and background, and “anthro + Bio + BG” represents the sum of simulated anthropogenic CO<sub>2</sub> enhancement, biological CO<sub>2</sub> enhancement and background.

emissions decreased by 37% during the COVID-19 control period when compared to the *posteriori* daily emissions between 2020 ( $12.10 \times 10^4$  tonnes) and 2019 ( $7.61 \times 10^4$  tonnes) in Nanchang city. The CO<sub>2</sub> emissions increased by 82% when comparing the 2021 with 2020 Level 1 period. Carbon dioxide emissions also increased by 14.3% between 2021 and 2019 Level 1 period. This indicates that economic activity quickly recovered to better than pre-pandemic conditions for the next year after strict control measures in 2020.

It should be noted that the MSF method only derived the change in total CO<sub>2</sub> emissions. The Bayesian inversion results can explore detailed optimization results for the main CO<sub>2</sub> categories (Table 1 and S4). To

understand the influence of *a priori* uncertainty combinations on the Bayesian *posteriori* emissions, we used different cases described above in Table S2. The results from these cases were averaged and the derived *posteriori* uncertainty represents the range of all combinations. To further evaluate whether these derived SFs for anthropogenic CO<sub>2</sub> emissions improved the CO<sub>2</sub> concentration simulations, we compared atmospheric CO<sub>2</sub> observations with simulations using both *a priori* and optimized CO<sub>2</sub> emissions (Fig. 5g–l). The results indicate that the bias in *a priori* CO<sub>2</sub> emissions was well calibrated with scatter plots closer to the 1:1 line. We also calculated the statistics for hourly midday CO<sub>2</sub> concentrations in the Level 1–3 period by using *posteriori* emissions. The

**Table 1**

Scaling factors and *posteriori* emissions by Bayesian inversion and Multiplicative scaling factor (MSF) method in years 2019, 2020 and 2021, units of CO<sub>2</sub> emissions × 10<sup>4</sup> tonnes CO<sub>2</sub>), ENE: power industry, IND: manufacturing combustion, Others: All anthropogenic CO<sub>2</sub> emissions except power industry and manufacturing combustion.

Method	Daily CO <sub>2</sub> emissions (× 10 <sup>4</sup> t CO <sub>2</sub> )	level 1 period			level 2–3 periods		
		2019	2020	2021	2019	2020	2021
Bayesian inversion	ENE	SF	1.17 (1.12–1.21)	0.53 (0.42–0.66)	1.33 (1.25–1.40) (0.57–0.77)	0.67 (0.76–0.85)	1.54 (1.43–1.63)
		<i>posteriori</i> (Nanchang)	5.98 (5.72–6.16)	2.72 (2.16–3.34)	6.74 (6.39–7.13) (2.83–3.80)	3.34 (3.84–4.29)	7.8 (7.19–8.11)
	IND	SF	0.94 (0.80–1.01)	0.76 (0.65–0.85)	0.94 (0.61–1.07) (1.22–1.47)	1.34 (0.96–1.00)	0.77 (0.61–0.89)
		<i>posteriori</i> (Nanchang)	1.64 (1.40–1.76)	1.33 (1.13–1.48)	1.63 (1.07–1.87) (2.13–2.54)	2.32 (1.67–1.72)	1.33 (1.06–1.54)
	Others	SF	1.15 (1.07–1.27)	0.86 (0.81–0.97)	1.45 (1.19–1.82) (1.24–1.49)	1.36 (1.02–1.16)	1.15 (1.11–1.14)
		<i>posteriori</i> (Nanchang)	3.35 (3.12–3.72)	2.51 (2.37–2.85)	4.22 (3.49–5.32) (2.90–3.48)	3.18 (2.38–2.70)	2.63 (2.59–2.67)
	All	<i>posteriori</i> (Nanchang)	10.97 (10.24–11.64)	6.56 (5.66–7.67)	12.58 (11.01–14.27)	8.84 (7.86–9.81)	11.62 (7.89–8.87)
	MSF	All	SF	1.24 (±0.09)	0.78 (±0.08)	1.42 (±0.10)	1.26 (±0.10)
	All	<i>posteriori</i> (Nanchang)	12.10 (±0.88)	7.61 (±0.78)	13.83 (±0.98)	11.42 (±0.91)	8.98 (±0.91)
							12.78 (±0.91)

RMSE, MB and R were 10.9 ppm, -3.0 ppm and 0.45 for 2019, 8.7 ppm, -1.3 ppm and 0.41 for 2020, and 13.0 ppm, -2.8 ppm and 0.38 for 2021. These results indicate that the *posteriori* emissions significantly improved the simulation of CO<sub>2</sub> concentrations when compared with the *a priori* emissions. In general, the overestimation of the *a priori* CO<sub>2</sub> simulations were largely scaled down during the COVID-19 pandemic (Fig. 5h). Further, the underestimation was also scaled up for the same period in 2021 (Fig. 5i).

Finally, we compared the optimization results by using both the MSF and Bayesian inversion approaches in Fig. 7. The Bayesian inversion method indicates that daily emissions decreased by 40.2% from 10.97×10<sup>4</sup> tonnes in 2019 to 6.56×10<sup>4</sup> tonnes in 2020 Level 1 period, and emissions in 2021 were 91.9% and 14.8% larger than year 2020 and 2019, respectively. Both methods are in general agreement (i.e. the relative differences are within 15%). However, there were some discrepancies between the MSF and Bayesian approach likely caused by the higher temporal resolution (hourly) of the Bayesian inversion approach. The MSF approach is based on the enhancement averages during a period and includes about 50 days in this study. However, we believe the derived relative changes using each method are generally comparable and physically reasonable. Further, we found that CO<sub>2</sub> emissions from power industry, manufacturing combustion and the remainder decreased by 54.5%, 18.9% and 25.1%, respectively, where power industry accounted for 73.9% of total CO<sub>2</sub> reductions. Our results indicate a large reduction of electricity and heat required for steel plants, paper mills, and other high energy consumption industries.

Although the local government reduced control measures from Level 1 to Level 2 since March 12th, 2020, and then continued to reduce it to Level 3 since March 20th, 2020, we found that CO<sub>2</sub> emissions in the Level 2–3 period increased by only 18.0% according to the MSF method and 26.1% according to the Bayesian inversion method when compared with the Level 1 period. Anthropogenic CO<sub>2</sub> emissions in Level 2–3 periods were substantially lower compared to the previous and following years. The *posteriori* results were 78.6% and 70.3% of emissions in 2019 and 2021, respectively for the MSF method and 93.6% and 71.2% when using the Bayesian inversion method. These results reflect the economy/industry activity and corresponding fossil fuel consumptions, which did not fully recover to normal conditions in Late March and April 2020.

#### 3.4. Implications for CO<sub>2</sub> emission from atmospheric CO observations

Because CO<sub>2</sub> and CO can be co-emitted by similar sources, the

atmospheric CO simulations can be used as a tracer to evaluate the SFs of CO<sub>2</sub>. The time series and diel averages for CO observations and CO simulations by using *a priori* CO emissions (default) are showed in Figs. 6 and 7. The simulated CO concentration is also displayed in Fig. 6 and S10, and Table S5. The simulations largely increased but some discrepancy was observed during the midday. The CO simulations were smaller than the observations in years 2019 and 2021 and higher in 2020. This discrepancy is similar to CO<sub>2</sub> as displayed in Fig. 5a–f. This problem is likely caused by the *a priori* emission bias and activity data. After we applied the SFs from CO<sub>2</sub> on CO emissions, the optimized simulation results for the five periods improved substantially as shown in Fig. S10, with midday simulated values in better agreement with the observations. The relatively good agreement when using SFs on CO emissions indicates the activity data bias was well calibrated.

#### 3.5. Emission reduction comparisons during COVID-19 period with previous studies

Many studies have applied different methods to quantify the influence of government control measures on anthropogenic CO<sub>2</sub> emissions in China or in other countries. For the studies in China, both bottom-up and top-down approaches were used. The CO<sub>2</sub> emission reduction rates concluded by different studies varied from 10% to 40% by four-fold among these studies, and by two-fold even with the same bottom-up approaches in China (Liu et al., 2020; Tohjima et al., 2020; Huang et al., 2021). Our results are consistent with Huang et al. (2021) who concluded that CO<sub>2</sub> emissions were reduced by 40% in east China by using activity data at city-level and specific sectors, and also agrees well with Tohjima et al. (2020) who found a 32% ± 12% reduction in China's anthropogenic CO<sub>2</sub> emissions in February and a 19% ± 15% reduction in March 2020. According to the report from the National Bureau of Statistics of China (NBSC, 2020), the total profit made by the Chinese industry sector decreased by around 40% during the first 3 months of 2020 when compared with 2019. This sharp decrease was mainly caused by production and also reflects fossil fuel consumption or CO<sub>2</sub> emission reductions from the power industry. Our results are slightly higher than another study, which conducted a global survey and showed that the CO<sub>2</sub> decreased by 21.8% in Jiangxi and around 20% for east China (Liu et al., 2020). By using GDP as proxy data, Han et al. (2020b) estimated that anthropogenic CO<sub>2</sub> emissions decreased by 11% in east China. As discussed above, such discrepancies can be caused by both uncertainty in proxy/activity data and the spatial mismatch. The comparisons of emission reduction rates with other countries indicate the difference in

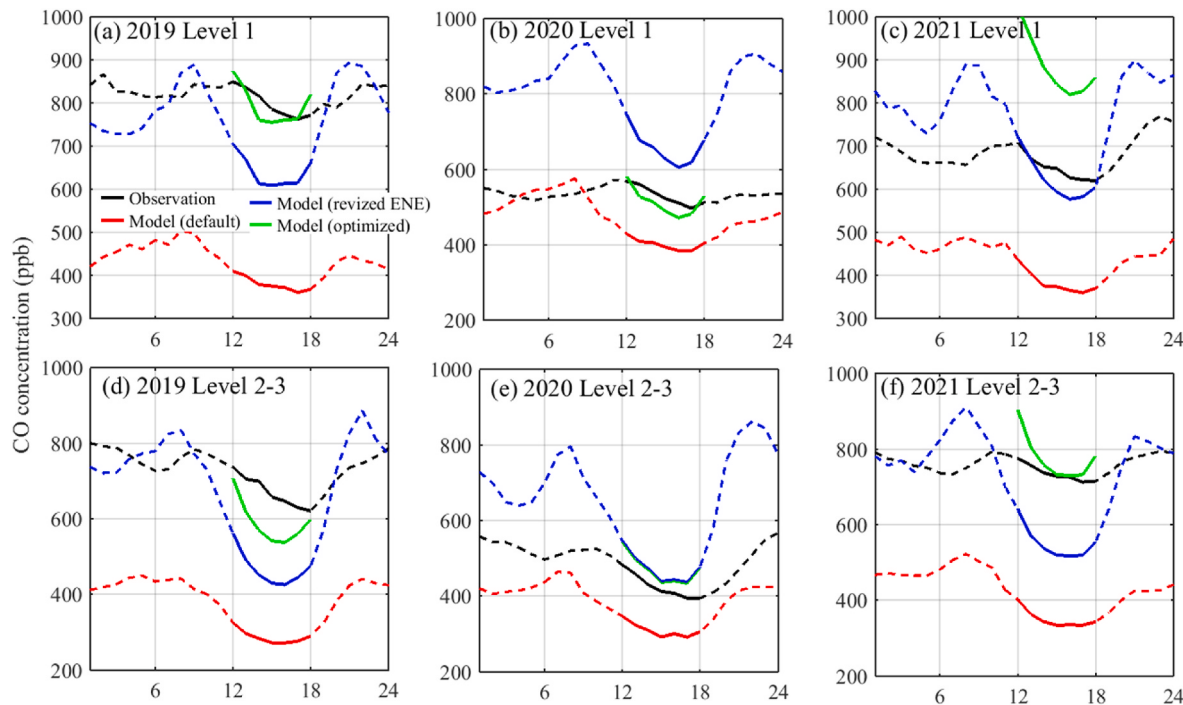


**Fig. 6.** Diel averages comparisons between observations and simulations in 2019, 2020 and 2021, midday (12:00–18:00, local time) values are displayed in bold lines. Here Model (default): the simulations using default EDGAR CO emission, Model (revised ENE): the used ENE CO emission is derived by the ENE CO<sub>2</sub> emission, Model (optimized): the SFs derived from CO<sub>2</sub> emissions are used to optimized CO emissions.

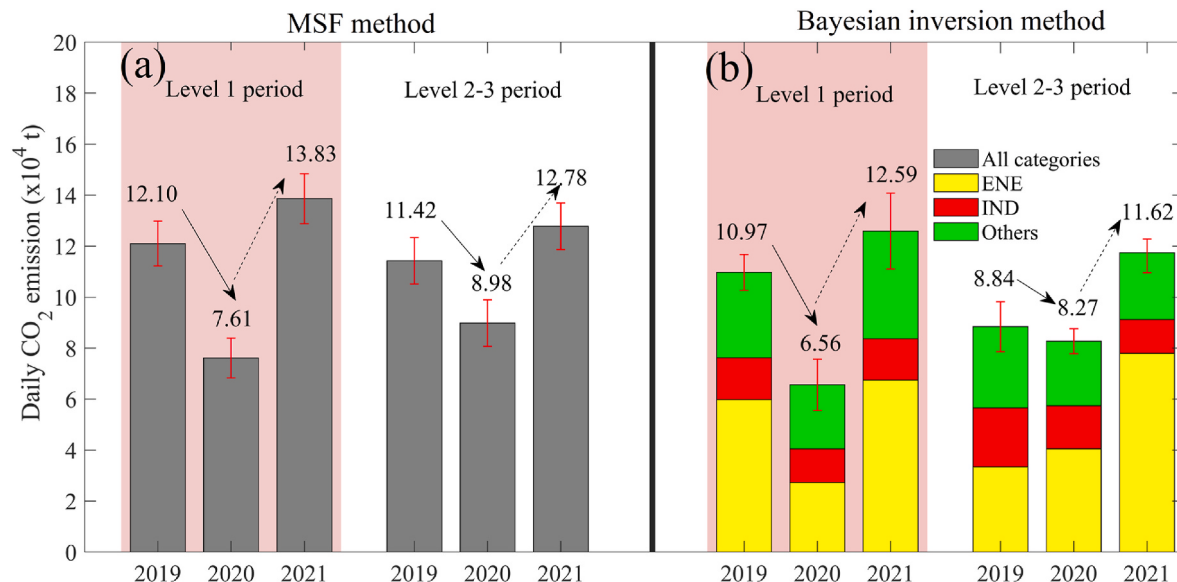


**Fig. 7.** Daily CO<sub>2</sub> emissions in Level 1 and Level 2-3 periods from 2019 to 2021 for Nanchang city, results of both (a) MSF method and (b) Bayesian inversion method are displayed, the red error bar illustrated the calculated uncertainty. (For interpretation of the references to color in this figure legend, the reader is referred to the Web version of this article.)

local control measures and fuel types. Comparisons with other countries are also discussed in Section S11.

Some studies have also analyzed air pollution reduction during COVID-19 in Jiangxi province. These pollutants (CO, NO<sub>x</sub>, SO<sub>2</sub>, and VOC) were reduced by 24%, 53%, 21%, and 43%, respectively (Wang et al., 2021). Further, the decline of emissions in other provinces around Jiangxi also showed similar reduction rates. Another recent study constrained urban NO<sub>x</sub> emissions in China by using satellite observations (Ding et al., 2020). They found NO<sub>x</sub> emissions were reduced by 20–50% for different cities during COVID-19 (January to March) and that

emissions from power plants were reduced by 40%. We should note that the strength of government control measures and regional fossil fuel consumption largely varied in different areas and countries. More tower-based observations would be helpful to resolve the spatial distributions of CO<sub>2</sub> emissions. However, there are still no tower-based CO<sub>2</sub> observation networks in China for any cities. Even a single tower observation system is relatively rare and only maintained in a few cities. The modeling framework used here has limitations associated with the assumptions of spatial distribution and source aggregation. We are relying on measurements from only one point in space. Consequently,

we cannot solve independently for the emissions from each model grid cell and time and individual source sector. This limitation has been acknowledged in other atmospheric inversion studies (Carouge et al., 2010; Bousquet et al., 2011; Chen et al., 2016). A denser atmospheric CO<sub>2</sub> observation network is needed to capture more spatially resolved emission signals.

#### 4. Conclusions

The COVID-19 pandemic provided a unique opportunity to evaluate the extent that anthropogenic CO<sub>2</sub> emissions can be reduced. Here, three years of atmospheric CO<sub>2</sub> measurements in Nanchang city, China were used to constrain CO<sub>2</sub> emissions. We found that the COVID-19 pandemic in 2020 reduced CO<sub>2</sub> emissions by 37.1–40.2% compared to the same period in 2019. Carbon dioxide emissions from the power industry (electricity and heat related power industry) and manufacturing industry decreased by 54.5% and 18.9% during the pandemic period. The power industry accounted for a 73.9% of the total CO<sub>2</sub> reductions, indicating that the large reduction of electricity was related to the reduced need for steel plants, paper mills, and other high energy consumption industries. We also found CO<sub>2</sub> emissions in 2021 were 14.3–14.9% larger than in 2019, indicating that economic activity quickly recovered to better than normal pre-pandemic conditions.

China has announced its goal to reach a CO<sub>2</sub> emission peak by 2030 and carbon neutralization by 2060. These ambitious goals should be based on full and accurate understanding of urban CO<sub>2</sub> emissions, which can account for 70% of total anthropogenic CO<sub>2</sub> emissions. However, recent studies that compared 9 different CO<sub>2</sub> inventories in China found that the relative difference of these inventories in China showed >50% bias from the province to city scale, thereby hindering the ability to assess the carbon neutralization goal. The atmospheric inversion approach is a powerful tool for constraining emissions and evaluating the uncertainty emission inventories. Our findings can serve as independent assessment of these urban CO<sub>2</sub> hotspots for both policy makers and the carbon cycle science community.

The atmospheric CO<sub>2</sub> observations data can be requested from Cheng Hu and Lingjun Xia, CO observation is provided by China National Environmental Monitoring Center (<http://datacenter.mep.gov.cn/>). EDGAR CO<sub>2</sub> and CO emission inventories can be downloaded from <http://edgar.jrc.ec.europa.eu/>, STILT model is downloaded from <http://www.stilt-model.org/>.

#### Author contribution

**Cheng Hu** designed the study, performed the model simulation, and wrote the original draft; **Lingjun Xia** conducted the atmospheric CO<sub>2</sub> observations. **Timothy J. Griffis** provided suggestions on the paper organization, writing, and improving the English grammar. All co-authors contributed to the data/figures preparation and analysis.

#### Declaration of competing interest

The authors declare that they have no known competing financial interests or personal relationships that could have appeared to influence the work reported in this paper.

#### Data availability

The data that has been used is confidential.

#### Acknowledgement

Cheng Hu is supported by the National Natural Science Foundation of China (grant no. 42105117), and the Natural Science Foundation of Jiangsu Province (grant no. BK20200802). Lingjun Xia is supported by the National Natural Science Foundation of China (grant no. 42105159).

Wei Xiao is supported by the National Key R&D Program of China (grants 2020YFA0607501& 2019YFA0607202).

#### Appendix A. Supplementary data

Supplementary data to this article can be found online at <https://doi.org/10.1016/j.envpol.2022.119767>.

#### References

- Basu, S., Lehman, S.J., Miller, J.B., et al., 2020. Estimating US fossil fuel CO<sub>2</sub> emissions from measurements of <sup>14</sup>C in atmospheric CO<sub>2</sub> [J]. *P. Natl. Acad. Sci. USA* 117 (24), 20191032.
- Bousquet, P., et al., 2011. Source attribution of the changes in atmospheric methane for 2006–2008. *Atmos. Chem. Phys.* 11 (8), 3689–3700. <https://doi.org/10.5194/acp-11-3689-2011>.
- Brunner, D., Kuhlmann, G., Marshall, J., Clément, V., Fuhrer, O., Broquet, G., Löscher, A., Meijer, Y., 2019. Accounting for the vertical distribution of emissions in atmospheric CO<sub>2</sub> simulations. *Atmos. Chem. Phys.* 19, 4541–4559. <https://doi.org/10.5194/acp-19-4541-2019>.
- Carouge, C., Peylin, P., Rayner, P.J., Bousquet, P., Chevallier, F., Ciais, P., 2010. What can we learn from European continuous atmospheric CO<sub>2</sub> measurements to quantify regional fluxes—Part 2: sensitivity of flux accuracy to inverse setup. *Atmos. Chem. Phys.* 8 (5), 3119–3129. <https://doi.org/10.5194/acp-8-18621-2008>.
- Chen, Z., et al., 2016. Partitioning N<sub>2</sub>O emissions within the US Corn Belt using an inverse modeling approach. *Global Biogeochem. Cycles* 30, 1192–1205.
- Ding, J., van der A, R.J., Eskes, H.J., Mijling, B., 2020. NO<sub>x</sub> emissions reduction and rebound in China due to the COVID-19 crisis *geophysical research letters*. *Geophys. Res. Lett.* (2), 1–9. <https://doi.org/10.1029/2020GL089912>.
- Fang, S.X., Zhou, L.X., Tans, P.P., Ciais, P., Steinbacher, M., Xu, L., Luan, T., 2014. In situ measurement of atmospheric CO<sub>2</sub> at the four WMO/GAW stations in China, *Atmos. Chem. Phys.* 14, 2541–2554. <https://doi.org/10.5194/acp-14-2541-2014>.
- Gensheimer, J., Turner, A.J., Shekhar, A., Wenzel, A., Keutsch, F.N., Chen, J., 2021. What are the different measures of mobility telling us about surface transportation CO<sub>2</sub> emissions during the COVID-19 pandemic? *J. Geophys. Res. Atmos.* 126, e2021JD034664 <https://doi.org/10.1029/2021JD034664>.
- Griffis, T.J., Chen, Z., Baker, J.M., et al., 2017. Nitrous oxide emissions are enhanced in a warmer and wetter world[J]. *Proc. Natl. Acad. Sci. USA*, 12081. <https://doi.org/10.1073/pnas.1704552114>.
- Gurney, K.R., Liang, J., Roest, G., et al., 2021. Under-reporting of greenhouse gas emissions in U.S. cities. *Nat. Commun.* 12, 553. <https://doi.org/10.1038/s41136-020-20871-0>.
- Guo, J., Zhang, J., Yang, K., Liao, H., Zhang, S., Huang, K., Lv, Y., Shao, J., Yu, T., Tong, B., Li, J., Su, T., Yim, S.H.L., Stoffelen, A., Zhai, P., Xu, X., 2021. Investigation of near-global daytime boundary layer height using high-resolution radiosondes: first results and comparison with ERA5, MERRA-2, JRA-55, and NCEP-2 reanalyses. *Atmos. Chem. Phys.* 21, 17079–17097. <https://doi.org/10.5194/acp-21-17079-2021>.
- Han, P., Zeng, N., Oda, T., Lin, X., et al., 2020a. Evaluating China's fossil-fuel CO<sub>2</sub> emissions from a comprehensive dataset of nine inventories. *Atmos. Chem. Phys.* 11371–11385. <https://doi.org/10.5194/acp-2019-643>.
- Han, P., Cai, Q., Oda, T., et al., 2020b. Assessing the recent impact of COVID-19 on carbon emissions from China using domestic economic data. *Sci. Total Environ.* 750, 141688 <https://doi.org/10.1016/j.scitotenv.2020.141688>.
- He, J., Naik, V., Horowitz, L.W., Dlugokencky, E., Thoning, K., 2020. Investigation of the global methane budget over 1980–2017 using GFIDL-AM4.1. *Atmos. Chem. Phys.* 20, 805–827. <https://doi.org/10.5194/acp-20-805-2020>.
- Hu, C., Xu, J., Liu, C., Chen, Y., Yang, D., Huang, W., Deng, L., Liu, S., Griffis, T.J., Lee, X., 2021. Anthropogenic and natural controls on atmospheric  $\delta^{13}\text{C}$ -CO<sub>2</sub> variations in the Yangtze River delta: insights from a carbon isotope modeling framework. *Atmos. Chem. Phys.* 21, 10015–10037. <https://doi.org/10.5194/acp-21-10015-2021>.
- Hu, C., Griffis, T.J., Liu, S., Xiao, W., Hu, N., Huang, W., Yang, D., Lee, X., 2019. Anthropogenic methane emission and its partitioning for the Yangtze River Delta region of China. *J. Geophys. Res.-Biogeosci.* 124 (5), 1148–1170.
- Huang, C., An, J., Wang, H., et al., 2021. Highly resolved dynamic emissions of air pollutants and greenhouse gas CO<sub>2</sub> during COVID-19 pandemic in east China. *Environ. Sci. Technol. Lett.* 8 (10), 853–860. <https://doi.org/10.1021/acs.estlett.1c00600>.
- Le Quéré, C., et al., 2020. Temporary decrease in daily global CO<sub>2</sub> emissions during the COVID-19 forced confinement. *Nat. Clim. Change* 10, 647–653. <https://doi.org/10.1038/s41558-020-0797-x>.
- Liu, Z., Ciais, P., Deng, Z., et al., 2020. Near-real-time monitoring of global CO<sub>2</sub> emissions reveals the effects of the COVID-19 pandemic. *Nat. Commun.* 11, 5172. <https://doi.org/10.1038/s41467-020-18922-7>.
- Miller, S.M., Matross, D.M., Andrews, A.E., Millet, D.B., Longo, M., Hirsch, A., Gerbig, C., Lin, J.C., Daube, B.C., Hudman, R., Leite da Silva Dias, P., Wofsy, S.C., 2008. Sources of carbon monoxide and formaldehyde in North America determined from high resolution atmospheric data. *Atmos. Chem. Phys.* 8, 7673–7696.
- Mueller, K.L., Lauvau, T., Gurney, K.R., et al., 2021. An emerging GHG estimation approach can help cities achieve their climate and sustainability goals. *Environ. Res. Lett.* 16, 084003, 2021.

- National Bureau of Statistics of China, 2020. Available online: [http://www.stats.gov.cn/english/PressRelease/202004/t20200428\\_1742015.html](http://www.stats.gov.cn/english/PressRelease/202004/t20200428_1742015.html). (Accessed 22 August 2021) (last access date: 2021)
- Oda, T., Haga, C., Hosomi, K., Matsui, T., Bun, R., 2021. Errors and uncertainties associated with the use of unconventional activity data for estimating CO<sub>2</sub> emissions: the case for traffic emissions in Japan. *Environ. Res. Lett.* 16 (8), 084058, 12pp.
- Paris, J.-D., Riandet, A., Bourtsoukidis, E., Delmotte, M., Berchet, A., Williams, J., Ernle, L., Tadic, I., Harder, H., Lelieveld, J., 2021. Shipborne measurements of methane and carbon dioxide in the Middle East and Mediterranean areas and the contribution from oil and gas emissions. *Atmos. Chem. Phys.* 21, 12443–12462. <https://doi.org/10.5194/acp-21-12443-2021>.
- Sargent, M., Barrera, Y., Nehrkorn, T., Hutyra, L.R., Gately, C.K., Mckain, K., Sweeney, C., Hegarty, J., Hardiman, B., Steven, C., Wofsy, S.C., 2018. Anthropogenic and biogenic CO<sub>2</sub> fluxes in the Boston urban region. *P. Natl. Acad. Sci. USA* 115 (40) https://doi.org/10.1073/pnas.1803715115.
- Seto, K.C., Dhakal, S., Bigio, A., Blanco, H., Delgado, G.C., Dewar, D., Huang, L., Inaba, A., Kansal, A., Lwasa, S., McMahon, J., Müller, D.B., Murakami, J., Nagendra, H., Ramaswami, A., 2014. Human settlements, Infrastructure and Spatial planning. *Climate Change 2014: Mitigation of Climate Change. IPCC Working Group III Contribution toAR5*. Cambridge University Press (Chapter 12).
- Tohjima, Y., Patra, P.K., Niwa, Y., Mukai, H., Sasakawa, M., Machida, T., 2020. Detection of fossil-fuel CO<sub>2</sub> plummet in China due to COVID-19 by observation at Hateruma. *Sci. Rep.* 10, 18688 <https://doi.org/10.1038/s41598-020-75763-6>.
- Turner, A.J., Kim, J., Fitzmaurice, H., Newman, C., Worthington, K., Chan, K., et al., 2020. Observed impacts of COVID-19 on urban CO<sub>2</sub> emissions. *Geophys. Res. Lett.* 47, e2020GL090037 <https://doi.org/10.1029/2020GL090037>.
- Wang, S., Zhang, Y., Ma, J., Zhu, S., Shen, J., Wang, P., Zhang, H., 2021. Responses of decline in air pollution and recovery associated with COVID-19 lockdown in the Pearl River Delta. *Sci. Total Environ.* 756, 143868 <https://doi.org/10.1016/j.scitotenv.2020.143868>.
- Wang, Y., Wang, X., Wang, K., et al., 2022. The size of the land carbon sink in China. *Nature* 603, E7–E9. <https://doi.org/10.1038/s41586-021-04255-y>.
- Weir, B., Crisp, D., O'Dell, C., et al., 2021. Regional impacts of COVID-19 on carbon dioxide detected worldwide from space. *Sci. Adv.* 7 eabf9415. <https://science.org/doi/10.1126/sciadv.abf9415>.
- Wu, S., Zhou, W., Xiong, X., Burr, G.S., Cheng, P., Wang, P., Niu, Z., Hou, Y., 2021. The impact of COVID-19 lockdown on atmospheric CO<sub>2</sub> in Xi'an, China. *Environ. Res.* 197, 111208 <https://doi.org/10.1016/j.envres.2021.111208>.
- Zavala-Araiza, D., Lyon, D.R., Alvarez, R.A., Davis, K.J., Harriss, R., Herndon, S.C., Karion, A., Kort, E.A., Lamb, B.K., Lan, X., Marchese, A.J., Pacala, S.W., Robinson, A. L., Shepson, P.B., Sweeney, C., Talbot, R., Townsend-Small, A., Yacovitch, T.I., Zimmerle, D.J., Ham-burg, S.P., 2015. Reconciling divergent estimates of oil and gas methane emissions. *P. Natl. Acad. Sci. USA* 112, 15597–15602. <https://doi.org/10.1073/pnas.1522126112>.
- Zeng N., Han P., Liu Z., et al., Global to local impacts on atmospheric CO<sub>2</sub> from the COVID-19 lockdown, biosphere and weather variabilities, *Environ. Res. Lett.* 17 015003 <https://doi.org/10.1088/1748-9326/ac3f62>.
- Zheng, B., Geng, G., Ciais, P., Davis, S.J., Martin, R.V., Meng, J., et al., 2020a. Satellite-based estimates of decline and rebound in China's CO<sub>2</sub> emissions during COVID-19 pandemic. *Sci. Adv.* 6 (49), eabd4998.
- Zheng, B., Zhang, Q., Geng, G., Chen, C., Shi, Q., Cui, M., Lei, Y., He, K., 2020b. Changes in China's anthropogenic emissions and air quality during the COVID-19 pandemic in 2020. *Earth Syst. Sci. Data* 13, 2895–2907. <https://doi.org/10.5194/essd-13-2895-2021>.